Rare Metal Materials and Engineering
Volume 55, Issue 4, April 2026
Available online at www.rmme.ac.cn

Science Press

Cite this article as: Guo Tingbiao, Li Yingying, Qian Danchen, et al. Micro-Nanostructured High-Strength and High-Conductivity Cu0.9Cr0.1Zr Alloy Prepared by C-ECAP, Cryogenic Rolling, and Aging[J]. Rare Metal Materials and Engineering, 2026, 55(04): 914-925. DOI: https://doi.org/10.12442/j.issn.1002-185X.20250223.

ARTICLE

Micro-Nanostructured High-Strength and High-Conductivity Cu0.9Cr0.1Zr Alloy Prepared by C-ECAP, Cryogenic Rolling, and Aging

Guo Tingbiao[1,2], Li Yingying[1], Qian Danchen[1], Deng Yang[1], Zhang Guoqing[1,2], Wang Yanfeng[3], Li Wenbing[3], Ling Dekui[3]

[1] State Key Laboratory of Advanced Processing and Recycling of Nonferrous Metals, Lanzhou University of Technology, Lanzhou 730050, China; [2] Key Laboratory of Non-ferrous Metal Alloys and Processing of Ministry of Education, Lanzhou University of Technology, Lanzhou 730050, China; [3] State Key Laboratory of Nickel and Cobalt Resource Comprehensive Utilization, Jinchang 737100, China

Abstract: The Cu0.9Cr0.1Zr alloy was deformed through continuous equal channel angular pressing (C-ECAP) through Route A, followed by liquid nitrogen cryogenic rolling (CR) and aging treated at 450 °C. The microstructure, mechanical properties, and conductivity of the alloy were detected by electron back-scattered diffractometer, energy dispersive spectroscope, X-ray diffractometer, scanning electron microscope, and transmission electron microscope. The evolution mechanism of the texture during the deformation process and its influence on mechanical properties were analyzed. The results show that directional shear bands form in the CuCrZr alloy during the C-ECAP process, and the preferred orientation of the microstructure is consistent with the rolling direction. After deformation, the number of precipitated phases (mainly Cr) increases with the prolongation of aging time, accompanied by the appearance of micro-nanostructured fibrous structure in the alloy. After C-ECAP for three passes, 75% CR deformation, and aging at 450 °C for 2 h, the tensile strength, microhardness, and conductivity reach 538 MPa, 168 HV, and 80%IACS, respectively. CR, aging heat treatment, and formation of recrystallization texture are all conducive to the improvement of conductivity.

Key words: C-ECAP; CR; aging heat treatment; precipitated phases; micro-nanostructure

1 Introduction

The high strength, high toughness, high electricity conductivity, and fine thermal stability of Cu and its alloys critically determine the performance of high-end electrical equipment in aviation, transportation, marine vessels, and other critical applications[1–4]. It is an urgent need in important fields such as communication, electricity, aviation, and high-speed railway catenary in recent years[5–7]. The low-energy states and coherent twin boundaries (TBs) not only severely restrict the slip and climb of dislocations during deformation, greatly improving the strength of the metal, but also have a negligible effect on the conductivity. Therefore, TB strengthening has become an important way to obtain high-strength and high-conductivity materials[8]. Many studies have found that the low-energy interfaces, such as TBs and low-angle grain boundaries (LAGBs), produced by plastic deformation of face-centered cubic (fcc) metals under ultra-high strain and low temperature conditions have better thermal and mechanical stability[9–11].

Studies have shown that equal channel angular pressing (ECAP) is an effective method for preparation of the ultrafine-grained, high-strength, and high-conductivity materials[12–14]. Guo et al[15] employed cryogenic ECAP on single-crystal copper, and revealed that oriented shear bands and high-density dislocations form within the single-crystal copper during processing. These mutually entangled dislocations effectively impede dislocation glide, thus enhancing the

Received date: April 29, 2025
Foundation item: Gansu Provincial Department of Education Industrial Support Program Project (2025CYZC-069); Central Government-Guided Local Science and Technology Development Fund Project (25ZYJE002); National Natural Science Foundation of China (51861022, 51261016)
Corresponding author: Guo Tingbiao, Ph. D., Professor, State Key Laboratory of Advanced Processing and Recycling of Nonferrous Metals, Lanzhou University of Technology, Lanzhou 730050, P. R China, E-mail: guotb@lut.edu.cn

tensile strength to 400.2 MPa while maintaining the intrinsic high electrical conductivity. Kováová et al[16] studied the effects of ECAP and heat treatment on the microstructure and mechanical properties of Cu-Cr-Zr alloy. The results showed that the mechanical properties of the alloy increase with the increase in aging temperature, and the best mechanical properties of the alloys are obtained by aging at 480 °C for 2 h. Wei et al[17] showed that after 4 passes of ECAP, 90% cold rolling deformation, and aging at 450 °C for 1 h, the tensile strength of Cu-0.5%Cr alloys is 554 MPa, the elongation at break is 22%, and the conductivity reaches 84%IACS, where IACS means international annealed copper standard. Through solid solution treatment, aging at 475 °C, and room-temperature ECAP, Chu et al[18] prepared a novel hetero-structure for Cu-1Cr-0.1Zr alloy, achieving synergistic enhancement of strength, ductility, and conductivity. The processed alloy exhibits ultimate tensile strength of 647 MPa, elongation of 15.9%, and electrical conductivity of 72.6%IACS. Su et al[19] found that cold deformation and aging treatment inhibit the dislocation diffusion, thus improving the strength and hardness of the alloys. And the precipitation of solute atoms reduces the degree of lattice distortion, which is beneficial to the recovery of conductivity of the alloy. Chen et al[20] found that the Cu/Cr interface suppresses the formation of dislocations during the heavy deformation process, which endows the CuCrZr alloy with higher strength and unchanged conductivity. Sousa et al[21] investigated Cu-Cr-Zr alloys processed by ECAP, aging, and rotary extrusion. ECAP refined grains to 0.7 μm in size, while aging promoted the formation of fine Cr- and Zr-rich precipitates. Their synergistic effect enhances both hardness and conductivity of the alloy. Route A is very effective in refining grains and generating high angle grain boundaries (GBs) and high-density dislocation, which are beneficial to increasing the strength and hardness of the material[22–23].

Deformation temperature, crystal orientation, and stacking fault energy are the key factors affecting the deformation twinning of metals[24]. Schuh et al[25] found that the appropriate segregation of alloying elements can improve the stability of GBs, which greatly regulates the strength of nano-metals. During the process, the formation of dispersed nano-precipitates and compounds after solution aging can further improve the strength and plasticity of the metal[26–27]. Therefore, the orientation and density of twins, dislocation configuration, and precipitated phases of Cu-Cr-Zr alloys can be adjusted by a combination of ultralow temperature plastic deformation and heat treatment[28].

However, traditional ECAP suffers from restricted sample lengths and microstructural inhomogeneity induced by frictional constraints and uneven deformation, thereby compromising material performance stability. Compared with conventional ECAP, continuous ECAP (C-ECAP) can significantly improve deformation homogeneity, enable continuous production of ultrafine-grained rods, enhance production efficiency, and demonstrate superior industrial viability. In this study, C-ECAP, cryogenic rolling (CR), and aging treatment were adopted for CuCrZr alloys prepared by Route A. Leveraging the synergistic effects of these processes, the evolution mechanisms of microstructure, conductivity, and mechanical properties of CuCrZr alloys during deformation were investigated.

2 Experiment

The experimental material used in this study was Cu0.9Cr0.1Zr (denoted as CuCrZr) alloy, which was subjected to homogenization annealing followed by solid solution treatment at 920 °C for 1 h+water cooling to obtain the coarse grain structure. Subsequently, the samples were deformed through Route A of C-ECAP at room temperature for 3 passes, resulting in a bar material of Φ9 mm×9 mm. Route A: after each deformation, the material is deformed in the original direction without any change. With the rotation of the extrusion wheel, the workpiece is continuously dragged into the extrusion die cavity through the friction force between the wheel groove and the workpiece to realize C-ECAP process. Maximum speed of ECAP extrusion wheel is 45 r/min, the diameter of extrusion wheel is 40 cm, and the rolling speed is 0.3 m/s. After C-ECAP, the samples were subjected to 25%, 50%, and 75% CR treatment, separately. To ensure the ultralow temperature conditions during rolling, each sample was presoaked in liquid nitrogen (−196 °C) for 3 min before each rolling pass. Subsequently, the samples underwent aging treatment at 450 °C for various durations. Fig. 1 shows the schematic diagram of C-ECAP and CR processes and the flow chart of Route A, in which ND, TD, and RD mean rolling direction, transverse direction, and normal direction, respectively.

Microstructure observations were performed in a thermal field emission scanning electron microscope (SEM, Quanta FEG-450) equipped with electron back scattered diffracto-meter (EBSD) with the step of 3 μm, a diffraction inclination of 70°, and acceleration voltage of 20 kV. Raw EBSD data were captured and post-processed using HKL Channel 5 and ATEX software. The distribution of elements and the structure of precipitated phases were examined by energy dispersive spectroscope (EDS). Transmission electron microscope (TEM, FEI Talos F200X) was used to further examine the mechanism of microstructure evolution. TEM samples were first mechanically ground until the thickness was approximately 50 μm and then thinned by a dual-jet polishing method. The electrolyte solution consists of 5vol% $HClO_4$+95vol% C_2H_5OH and is controlled at −30 °C with liquid nitrogen. Macroscopic texture characterization was performed by X-ray diffractometer (XRD, D8ADVANCE) with a scanning angle of 10°–100° and a scanning speed of 2°/min.

Mechanical properties were evaluated by measuring the tension at a constant tensile rate of 0.5 mm/min using a WDW100-D testing machine. The microhardness of the alloy was tested by HV-1000 microhardness tester, and 5 points were hit equidistantly from the center to the edge on the surface of the sample. The average value was taken as the microhardness value. Using the Sigma 2008B/C digital eddy

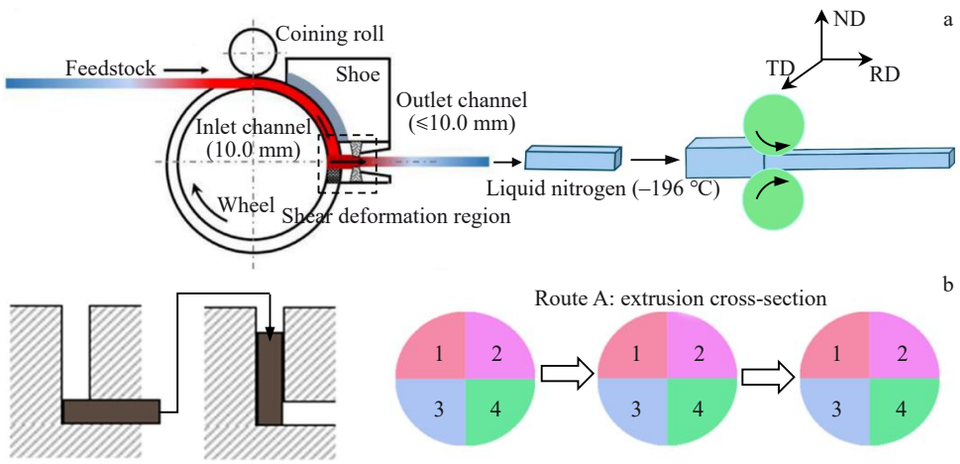

Fig.1 Schematic diagram of C-ECAP and CR processes (a); flow chart of Route A (b)

current metal conductivity meter, the conductivity of different samples was measured at room temperature in IACS unit. The higher the IACS value, the better the conductivity. At least 5 different points were measured for each sample, and the average of these measurements was calculated to obtain the final result.

3 Results and Discussion

3.1 Deformation microstructure

Fig. 2 shows EBSD results of CuCrZr alloy after C-ECAP and 75% CR. It can be seen that after C-ECAP via Route A combined with 75% CR deformation, the grain orientation is mainly along the (101), with an average grain size of 0.41 μm, reaching the nanometer level. C-ECAP process can refine the grains of alloys, and combined with CR, the grains are further refined and their sizes become more uniform[29]. The value of Schmid factor is small, which is due to the strain increasing during the C-ECAP and CR processes, the uniform grain refinement, and the increasing dislocation density. The dislocation tangles with each other hinder their movement, and the slip is not easy to occur. Fig. 2g presents the pole figures of CuCrZr alloy after deformation, it can be observed that the strongest orientation is in the {100} and {111} families of crystal planes, with an extreme density of 6.94.

The analysis shows that the alloys subjected to C-ECAP with CR in liquid nitrogen result in uniform grain fragmentation and are easy for rotation. Most of the grains show preferential orientation in {111} family of crystal planes under high strain, the structure is more uniform, and the extreme value of the density is smaller.

Fig. 3 shows XRD patterns of the CuCrZr alloy after 3 passes of extrusion in C-ECAP through Route A followed by CR with different reduction. It can be seen that when CR reduction reaches to 25%, the diffraction intensity of (111) crystal plane decreases the most, and the diffraction intensity of the (200) plane increases the most. The diffraction intensity of (220) and (311) crystal planes increases slightly, and the preferred orientation is still in (111) crystal plane. The diffraction intensity of both (111) and (200) crystal planes decreases when CR reduction reaches to 50%, with a large decrease in (111) crystal plane and a large increase in diffraction intensity of (220) crystal plane, and the preferred orientation is in (220) crystal plane. When CR reduction reaches to 75%, the diffraction intensity in (111) and (200) crystal planes continues decreasing, with a small diffraction peak of (111) crystal plane and an increase in diffraction intensity of (220) crystal plane, and the preferred orientation is still in (220) crystal plane.

Fig. 4 shows the Schmid factor and average grain size of CuCrZr alloy prepared by C-ECAP through Route A, CR, and aging at 450 °C for 1 h. The Schmid factor is an important parameter to describe the plastic deformation of the crystal, which quantifies the possibility of a specific slip system in the crystal to move under the action of a given external force. The higher the Schmid factor, the greater the probability of the slip system initiation, i. e., the higher the probability of plastic deformation of the material. From Fig.4a, 4c, and 4e, it can be seen that the Schmid factor values of {100} and {101} are increased after 25% CR and aging, and the slip system of {100} crystal plane slips preferentially. After 50% CR and aging, the Schmid factor value decreases. The Schmid factor increases and then decreases with the increase in CR reduction. At the beginning of deformation, as the strain increases, the grains elongate and are refined along the deformation direction, which leads to the orientation of some grains more favorable to the activation of the slip system, resulting in the initial increase in Schmid factor. During the deformation process, strain continuously accumulates, grains further fragment, and the distribution of orientations becomes complex. Additionally, the increase in dislocation density makes slip less favorable, leading to a decrease in Schmid factor. After 75% CR and aging, the internal storage energy of the alloy is large under high strain, and recrystallization is easy to occur during aging. At the same time, grain breakage and rotation are also conducive to the activation of the slip system. With the increase in deformation reduction, the grains gradually become elongated and fragmented noticeably along

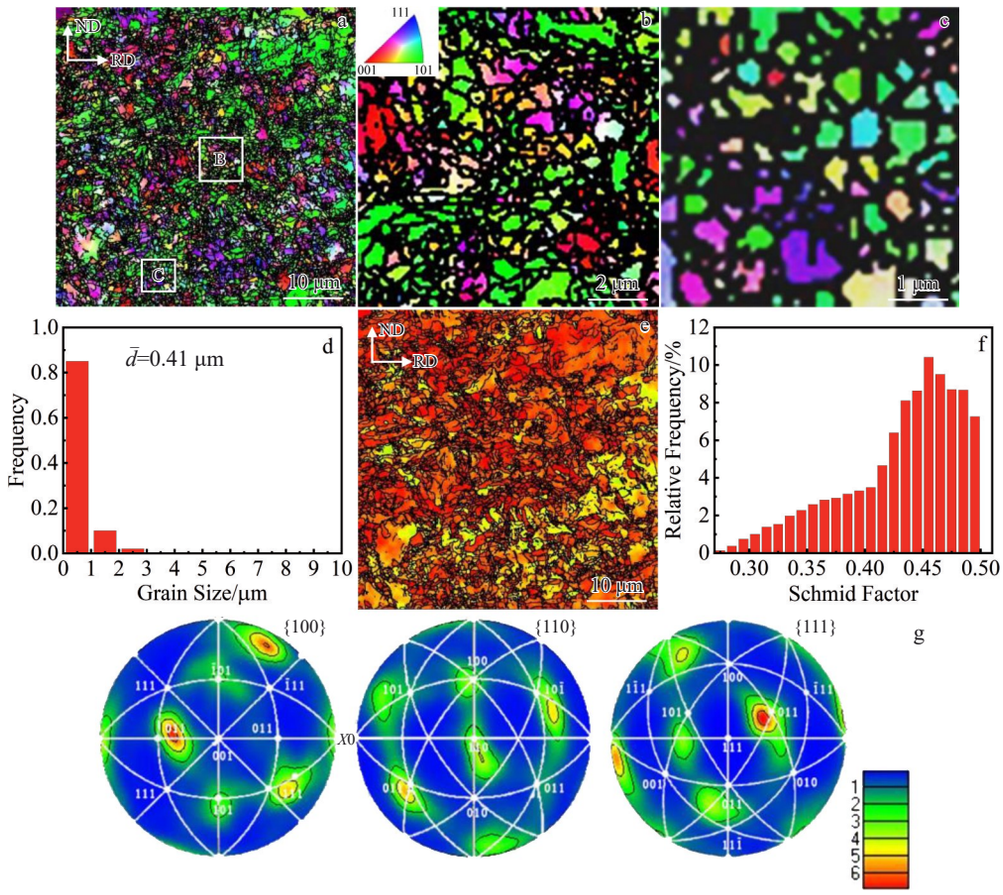

Fig.2 EBSD results of CuCrZr alloy prepared by C-ECAP through Route A and CR: (a) GB map; (b) enlarged image of region B marked in Fig.2a; (c) enlarged image of region C marked in Fig.2a; (d) distribution of grain size; (e) Schmid factor map; (f) statistical result of Schmid factor; (g) pole figures

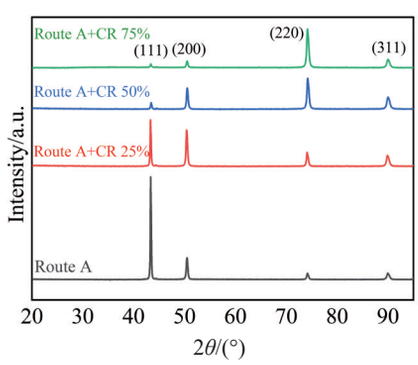

Fig.3 XRD patterns of CuCrZr alloys prepared with different CR reduction

the direction of deformation, making the GBs indistinct. This process promotes the formation of micro-nano fibrous structures within the CuCrZr alloy. Fig. 4b, 4d, and 4f show the grain size and contrast map of the alloy. It can be found that after 25% CR, the grains elongate along the rolling direction, and the average grain size is about 0.77 μm. After reduction reaches 50%, the grains are continuously refined, the average grain size is 0.66 μm, and more than 80% of the grains are refined to less than 1 μm in size. After CR reduction reaches 75%, the grains continue to refine under large deformation, the average grain size reaches 0.53 μm, and the proportion of grains with size below 1 μm continues to increase.

3.2 Recovery and recrystallization

Fig.5 shows the recrystallization microstructure of the alloy after C-ECAP, CR, and aging at 450 °C for 1 h. It can be found that when the deformation reduction reaches to 25%, sub-grain structure accounts for more proportion, and the analysis shows that the grain fragmentation has possibly produced a large number of sub-grains. The percentage of deformed grains increases when the deformation reduction reaches to 50%. When the deformation reduction is 75%, higher energy storage in the grains at high strain leads to the faster recovery process and the increase in recrystallized grains.

Fig.6 shows XRD patterns of CuCrZr alloy after C-ECAP, 75% CR, and aging at 450 °C for various durations. It can be seen from Fig. 6a that as aging time is prolonged, the diffraction intensity of the main diffraction peak (220) increases first and then decreases, and the diffraction intensity of diffraction peak (311) increases slightly. By analysis, the storage energy in the alloy increases during CR, and the

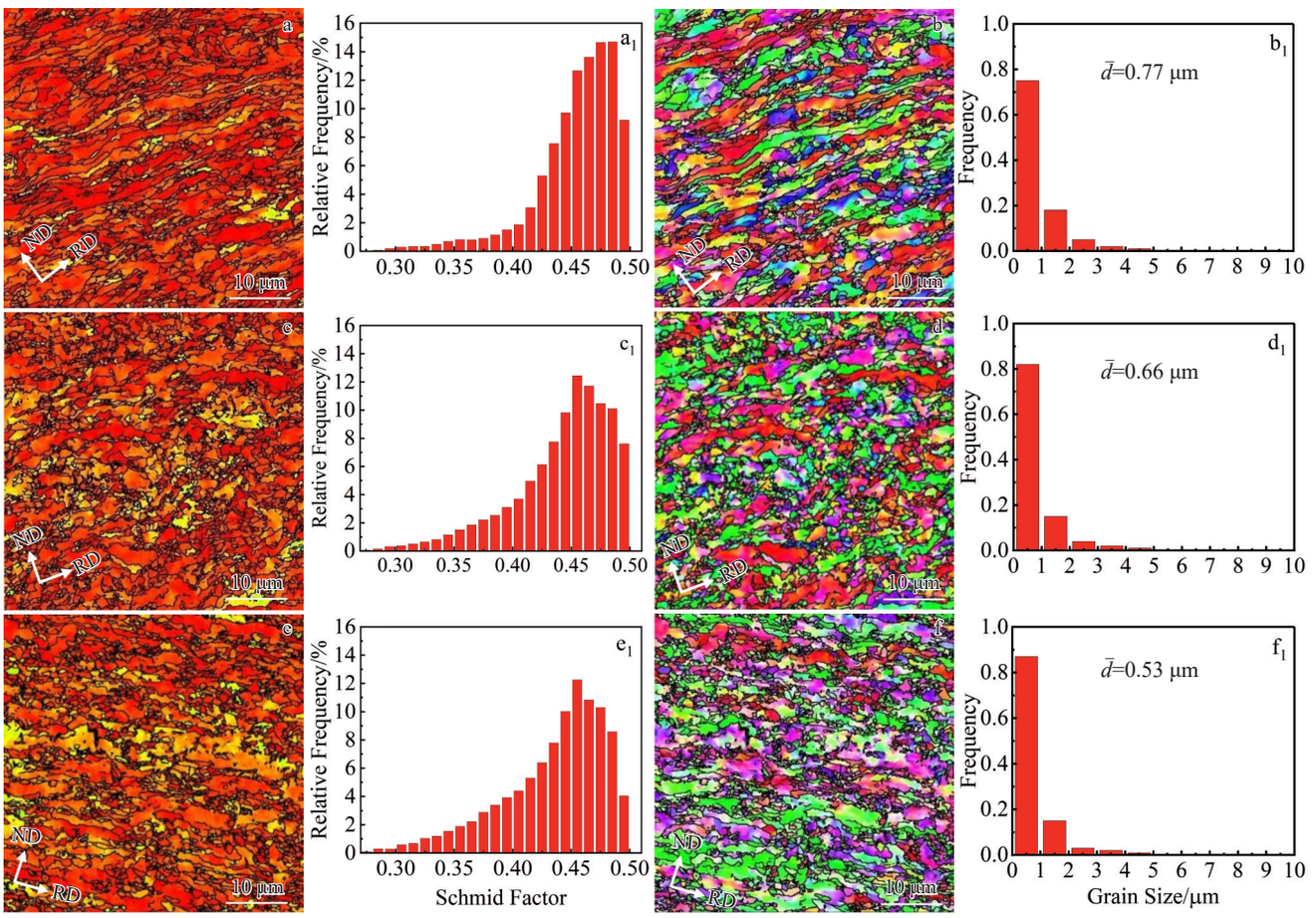

Fig.4 Schmid factor analyses (a–a_1, c–c_1, e–e_1) and grain size distributions (b–b_1, d–d_1, f–f_1) of CuCrZr alloy after C-ECAP, CR with different reduction, and aging at 450 °C for 1 h : (a–b, a_1–b_1) 25%; (c–d, c_1–d_1) 50%; (e–f, e_1–f_1) 75%

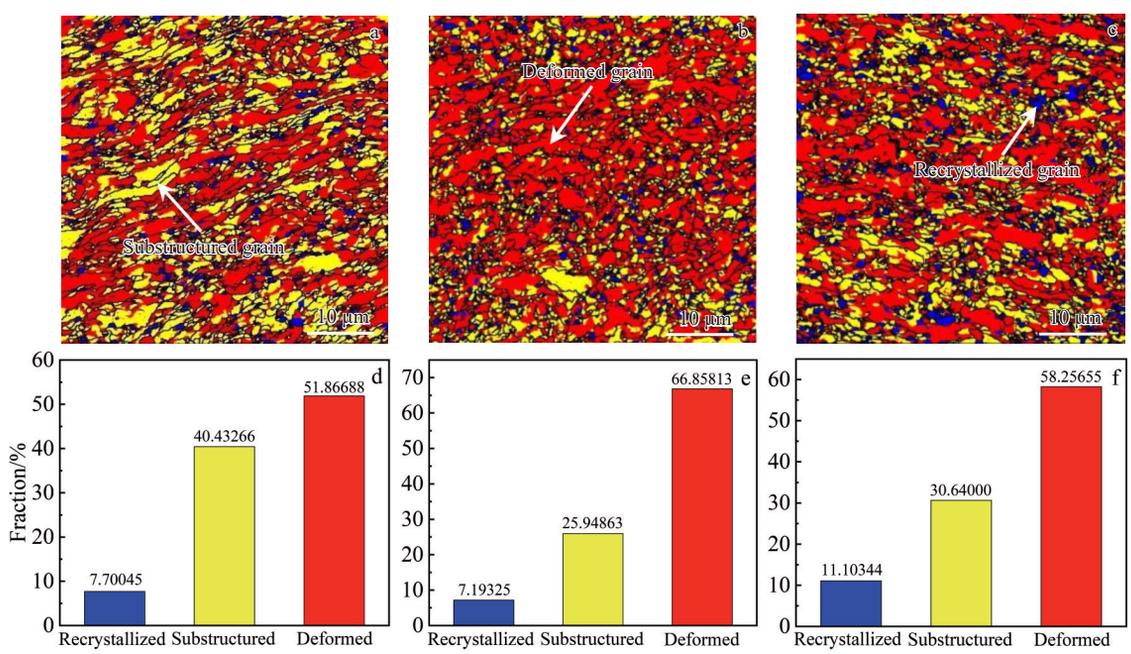

Fig.5 Grain distribution maps (a–c) and corresponding statistical results (d–f) of CuCrZr alloy after C-ECAP, CR with different reduction, and aging at 450 °C for 1 h: (a, d) 25%; (b, e) 50%; (c, f) 75% (the yellow part is substructured grain, the blue part is recrystallized grain, and the red part is the deformed grain)

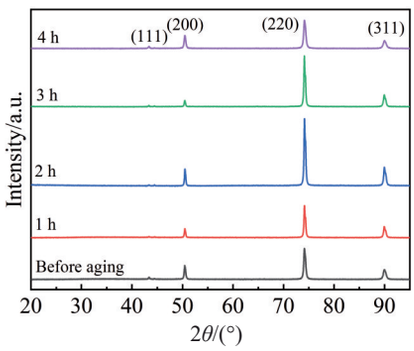

Fig.6 XRD patterns of CuCrZr alloys after C-ECAP, 75% CR, and aging at 450 °C for different durations

precipitated phase precipitates continuously during the aging process. The different dislocations on the same slip boundary offset each other and the slip resistance decreases, which result in the increase in diffraction intensity of the (220) with the prolongation of aging time. In the later stage of aging process, the main slip (220) is blocked, the number of slip systems increases, and partial cross slip occurs. The sub-slip boundary (311) is activated, and the diffraction intensity increases.

3.3 Orientation distribution

Fig.7 is the misorientation distributions of the CuCrZr alloy after C-ECAP by Route A, CR, and aging at 450 °C for 1 h. It can be seen from Fig.7 that under the same aging conditions, the proportion of LAGBs increases first and then decreases as the rolling strain increases. The size of the sub-grain reaches the micron level when the CR reduction is 25%. With the increase in CR reduction, some large grains continue to break. Under high strain, dislocation proliferation leads to the increase in dislocation density. The dislocation walls near the GBs absorb dislocations and are reorganized into sub-grain boundaries. During the aging process, solid solution atoms precipitate on GBs and pin the GB, so the proportion of LAGBs remains unchanged.

Fig. 8 shows the pole figures of the CuCrZr alloy after C-ECAP, CR with different reduction, and aging at 450 °C for 1 h. As depicted in Fig. 8a, the preferred orientation achieved through CR with a 25% reduction and subsequent aging is towards the {100} family of crystal planes. Upon increasing the reduction to 50%, because of the increased deformation, the strain increases and the texture is more concentrated, with the strongest orientation near {111} and an extreme density of 4.65. Further increasing the reduction to 75% leads to a shift in the strongest orientation towards a combination of {111} and {110} families of crystal planes. CR continues to refine grains, and the extreme density of the texture increases to 8.04, signifying a continuous concentration of the texture throughout the process. Clearly, in addition to the preferred orientation, there are other textures. However, the extreme density of these textures is relatively low, and its impact on the alloy performance is small. Extreme density can indicate the degree of homogenization of the microstructure. The more dispersed the microstructure, the smaller the extreme density. And the more concentrated the microstructure, the larger the extreme density. As can be seen from the changes in alloying preferences, when the amount of deformation is small, different grains rotate along the preferential orientation and the polar density increases. Following higher strain and subsequent aging, the texture becomes more concentrated and the extreme density further increases. This is because CR is more homogeneous and the sub-grains tend to rotate, leading to concentration of the texture.

Fig. 9 displays the orientation distribution function (ODF) maps of CuCrZr alloys after C-ECAP, CR with different reduction, and aging at 450 °C for 1 h. It can be seen that there are large differences in the texture strength depending on the rolling deformation, but the type of texture is basically the same. By comparing with the common spatial cross section of the cubic crystal system[30], it is observed that after 25% CR, the φ_2=0° cross section exhibits both {001} and {110} textures, while the φ_2=45° cross section reveals the presence of {001} and {110} textures. After 50% CR, there is a weak texture near {110} in the cross section with φ_2=0°, and the textures on the cross section with φ_2=45° gather near {110} and {112}. After 75% CR, the texture gathers near {110} in the cross section with φ_2=0°. There are {001} texture and {110} texture on the cross section with φ_2=45°, and the texture

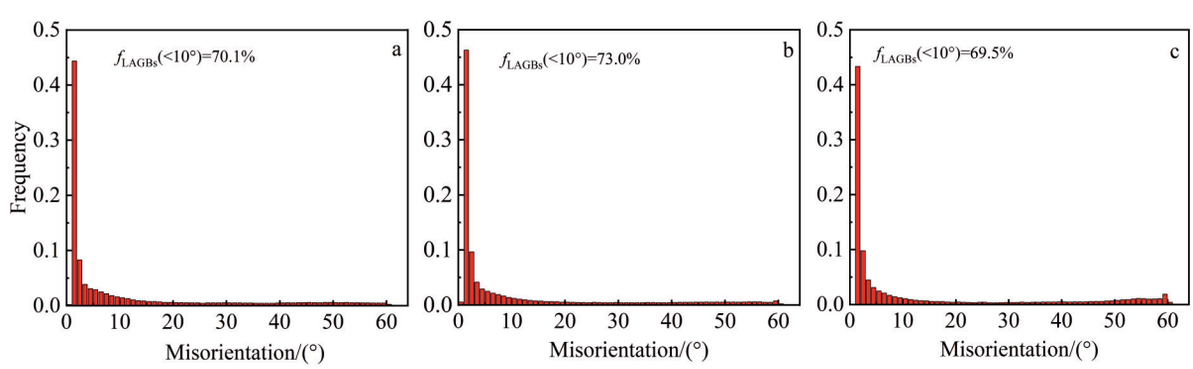

Fig.7 GB misorientation distributions of CuCrZr alloy after C-ECAP, CR with different reduction, and aging at 450 °C for 1 h: (a) 25%; (b) 50%; (c) 75%

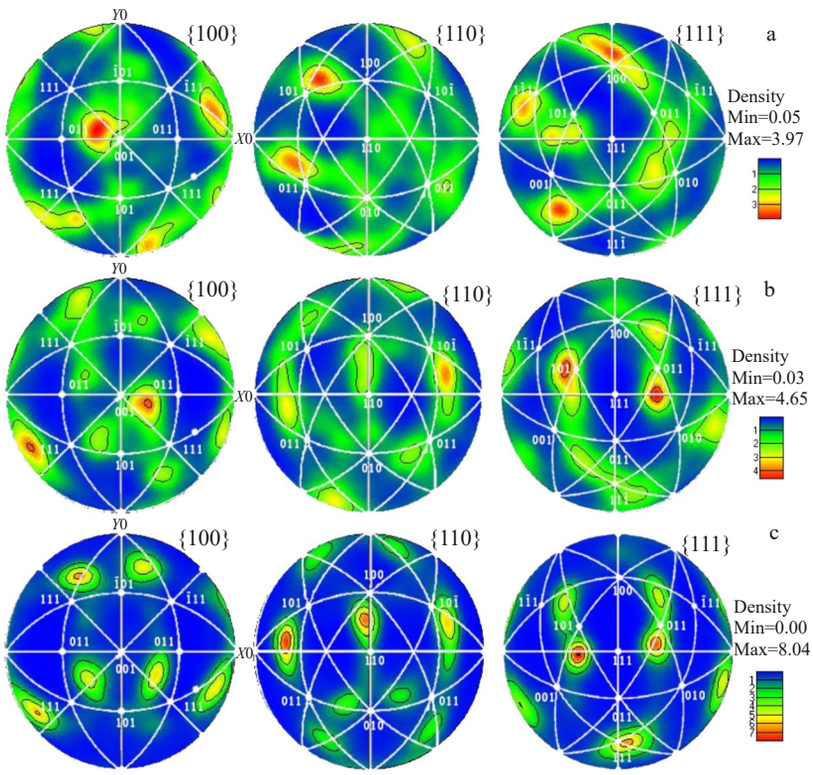

Fig.8 Pole figures of CuCrZr alloys after C-ECAP, CR with different reduction, and aging at 450 °C for 1 h: (a) 25%; (b) 50%; (c) 75%

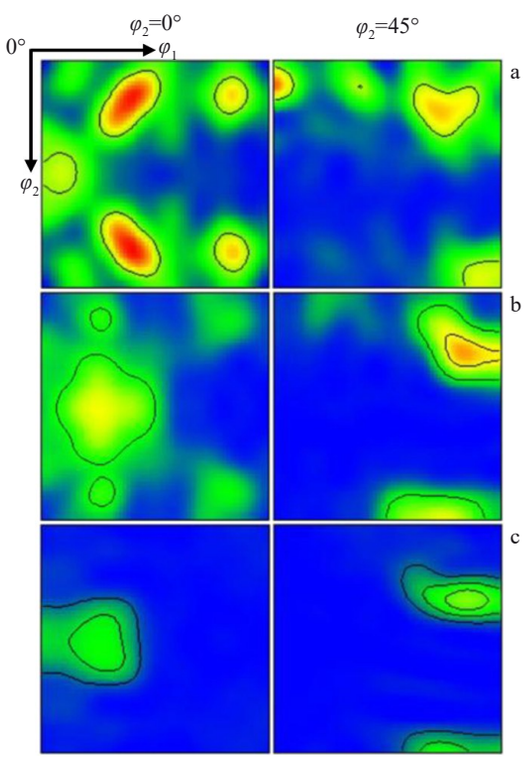

Fig.9 ODF maps of CuCrZr alloys after C-ECAP, CR with different reduction, and aging at 450 °C for 1 h: (a) 25%; (b) 50%; (c) 75%

is obviously aggregated. The texture intensity increases with the increase in CR reduction, and the maximum texture intensity is 14.8 when the CR reduction is 75%.

Under the same aging conditions, the texture distribution and intensity on different sections change with the increase in CR reduction. The basic types of texture are both {001} and {110}. The {110} texture is of great significance for the strength improvement of the CuCrZr alloy, while the {001} texture is conducive to the transmission of electrons in the lattice, and plays a positive role in the recovery of conductive performance as well as the enhancement in plasticity of alloy.

3.4 Precipitation behavior

Fig. 10 shows EDS scanning results of the alloys after C-ECAP, CR with different reduction, and aging at 450 °C for 1 h. It is considered that the granular phases consist of elements Cr and Zr, which precipitate uniformly in the matrix. The precipitation of element Zr can inhibit the growth of Cr precipitated phases and promote the aggregation and precipitation of element Cr in the matrix, thus promoting the uniform distribution of the precipitated phase in the copper matrix. During the movement of dislocations, the homogeneous and fine precipitated phases play a role in hindering and pinning the dislocations, and the continuous movement of dislocations requires more energy to support, which results in the precipitation strengthening and improved properties. With the increase in CR reduction, the storage energy of alloy increases. Under the same aging condition, the higher the strain, the more the precipitates.

Fig.11 shows TEM images of CuCrZr alloys after C-ECAP, CR, and aging at 450 °C for 1 h. After CR, the grains are elongated along the direction of the shear band, ultimately

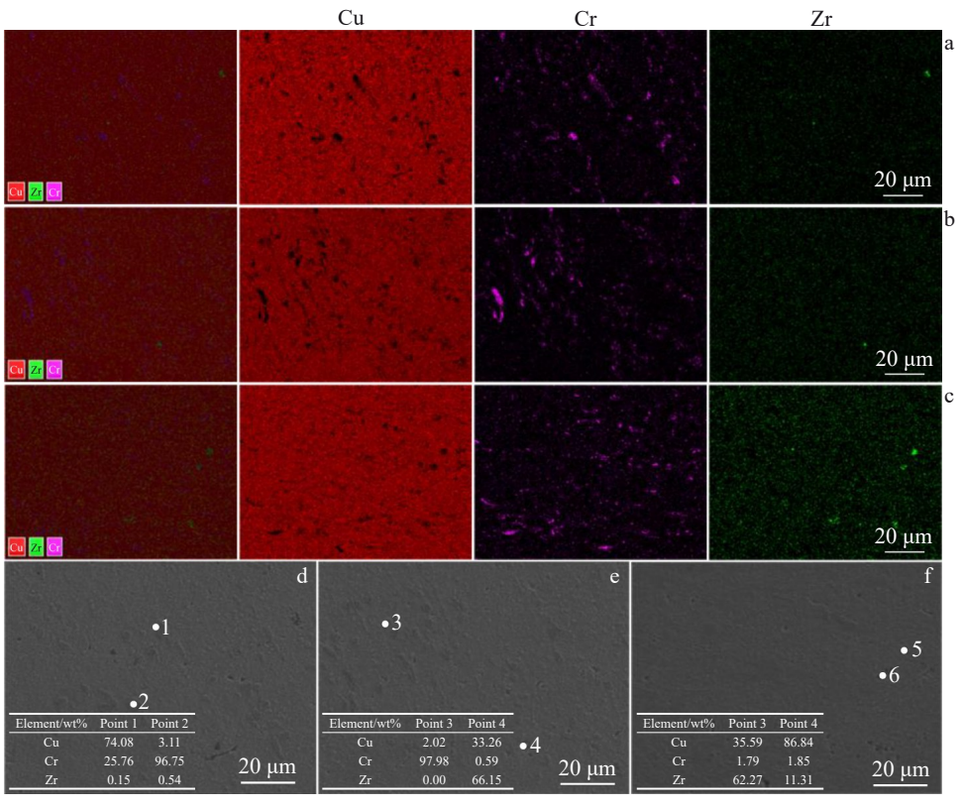

Fig.10 EDS scanning results of CuCrZr alloys after C-ECAP, CR with different reduction, and aging at 450 °C for 1 h: (a, d) 25%; (b, e) 50%; (c, f) 75%

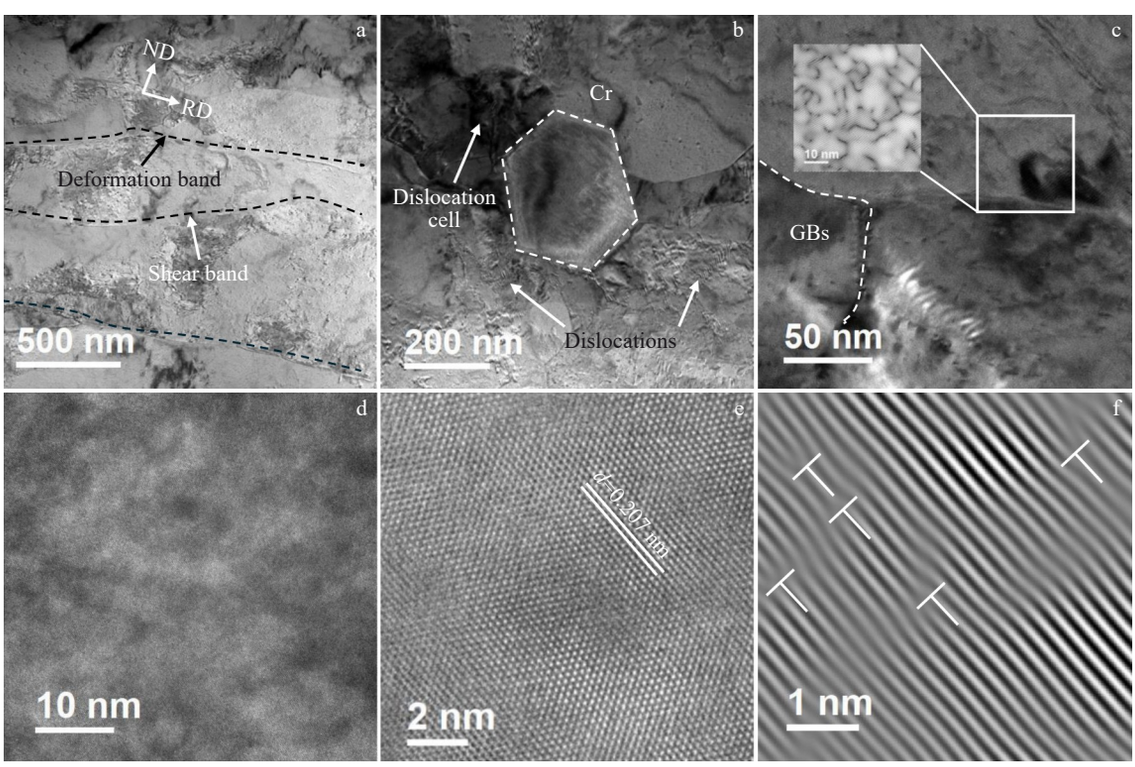

Fig.11 TEM images at different magnifications of CuCrZr alloy after C-ECAP, CR of 75%, and aging at 450 °C for 1 h

forming strip-like grains and laminar deformation bands, as shown in Fig. 11a. Throughout the entire CR process, the dislocations continue to increase, which improves the plasticity of material. Fig. 11b illustrates that there exists a

precipitated phase, which is obviously different from the matrix. EDS analysis of the precipitated phase indicates that there is a high Cr content. In conjunction with SEM results, it can be judged that the precipitated phase is Cr, with a diameter of about 250 nm. In the process of continuous deformation, with the increase in stress, the alloy undergoes significant strain. Driven by the energy differential among atoms at various locations, the structure at these sites becomes more susceptible to instability, which leads to the accumulation of precipitate-forming elements and the subsequent formation of precipitated phase.

As shown in Fig.11b, dislocations of extremely high density exist near the precipitate phase. This is attributed to the distribution of the secondary phase particles in the matrix, which impedes the movement of dislocation, leading to dislocation pile-ups and consequently enhancing the strength of material. The presence of solute atoms increases the scattering rate of electrons, which leads to a significant decrease in conductivity of the material. After CR, the number of solute elements in the matrix decreases with the precipitation of element Cr, which has an important effect on the recovery of the conductivity. In addition, with the increase in reduction during CR process, the dislocation density within the grain increases. Dislocations produce successive reactions during slip, and a large number of dislocations are entangled with each other, forming sub-grain boundaries, as shown in Fig. 11c. The existence of sub-grain boundaries impedes the dislocation movement. At the same time, the grains that firstly undergo plastic deformation are constrained by the surrounding grains, and coordinated motion between grains leads to a significant improvement in the mechanical properties of the alloy. From high-resolution TEM image, it can be seen that there are a large number of dislocations in the matrix, which is consistent with the previous analysis.

3.5 Mechanical properties and conductivity

Fig. 12 shows the changes in tensile strength, microhardness, elongation, and conductivity of the CuCrZr alloy at different processing stages. It can be seen that the mechanical properties of the alloy have been significantly improved after CR. As depicted in Fig. 12a – 12b, when CR reduction reaches to 75%, the tensile strength reaches to 542 MPa, which is 24.3% higher than that before CR. Similarly, the microhardness value rises to 146 HV, representing a increase of 11.8% compared to that before CR. The elongation of the alloy is shown in Fig. 12c. An analysis reveals that as reduction increases, the overall trend in elongation is downward, with elongation values after CR being lower than that before CR. The lowest elongation recorded for alloy after CR is 11.5%. Fig. 12d shows the conductivity of CuCrZr alloy after 75% CR increases to 47.4%IACS.

During CR, the tensile strength and microhardness of the alloy increase with the increase in strain. This is because during deformation at low temperature (– 196 °C), the energy stored in the alloy cannot meet the needs of diffusion. The dislocations accumulate and Cottrell atmosphere pinning is easy to occur in the alloy, which leads to an increase in deformation resistance and a strong work hardening effect during the process. With the increase in strain, precipitated phases with different sizes (Cr, Zr, and Cu-Cr and Cu-Zr compounds) precipitate along the GBs as the dislocations diffuse and are entangled, impeding the movement of dislocations and increasing the tensile strength

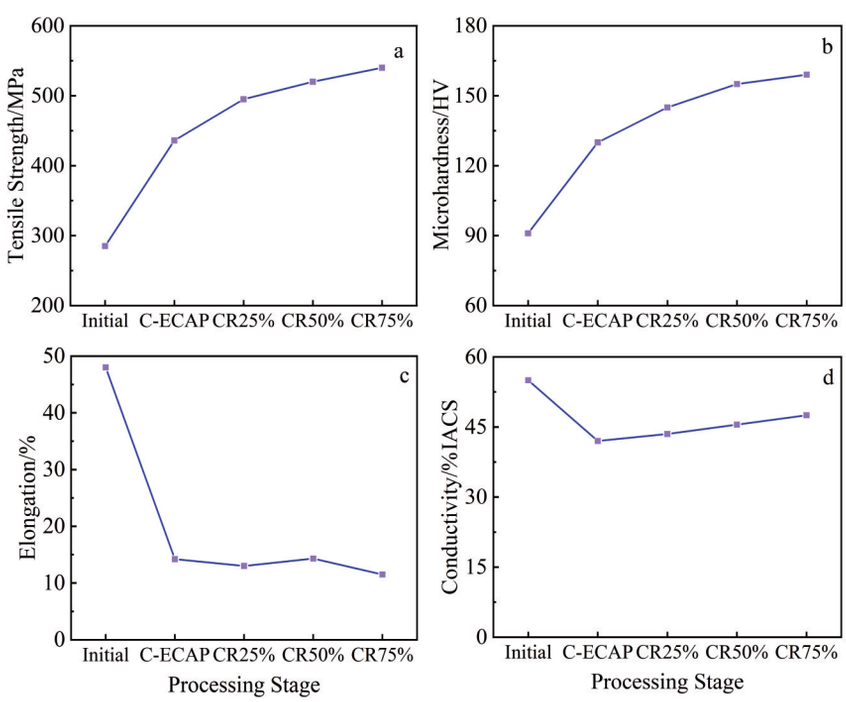

Fig.12 Mechanical properties of CuCrZr alloys at different processing stages: (a) tensile strength; (b) microhardness; (c) elongation; (d) conductivity

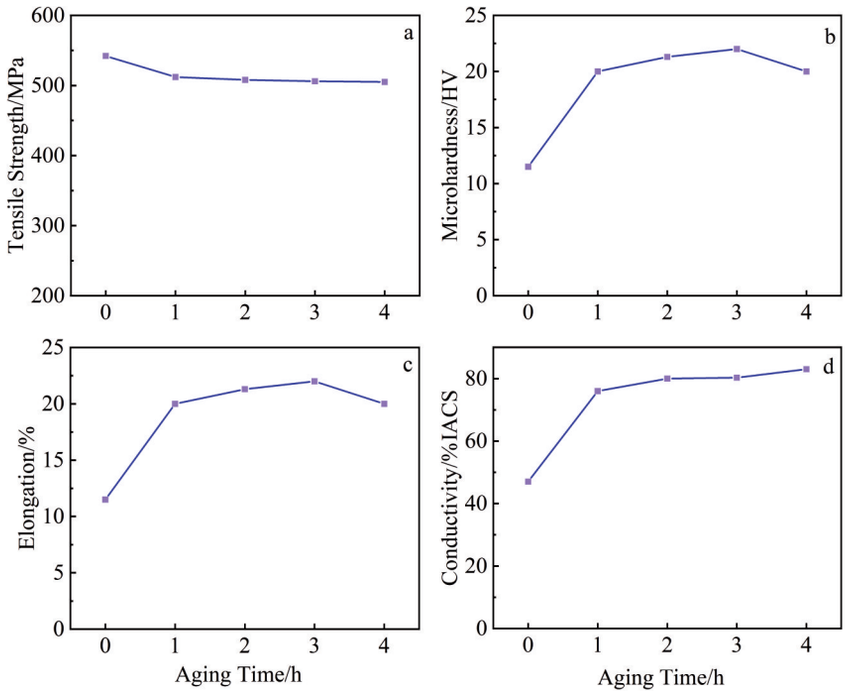

Fig.13 Mechanical properties of CuCrZr alloys after C-ECAP, CR with reduction of 75%, and aging at 450 °C for different durations: (a) tensile strength; (b) microhardness; (c) elongation; (d) conductivity

and mcirohardness of the alloy[31]. When CR reduction reaches to 75%, the dislocation proliferation and mutual offset achieve a dynamic balance. After CR, the work hardening and fine-grain strengthening are the main strengthening mechanisms. The subsequent CR process can eliminate the defects, such as vacancies within the alloy, enhance the density, and consequently improve the conductivity of the alloy[32].

The mechanical properties of the CuCrZr alloy after C-ECAP, CR, and aging at 450 °C for different durations are shown in Fig. 13. It can be seen from Fig. 13a that with the prologation of aging time, the tensile strength of the alloy increases first and then decreases. The maximum tensile strength of the alloy is 537 MPa, and the microhardness of the alloy reaches to 168 HV after aging at 450 °C for 2 h. After aging for 4 h, the tensile strength and microhardness decrease significantly. The analysis results show that with the prolongation of aging time, the amount of the precipitates increases, precipitates grow up, and the recrystallization rate continuously increases, leading to softening of the alloy and the decrease in mechanical properties. The variation in elongation of the alloys is shown in Fig. 13c. It can be seen that with the prolongation of aging time, the elongation of the alloys increases in general. The elongation of the alloy increases most significantly within the first 0 – 1 h, and remains basically stable between 1 – 4 h. After aging for different durations, the elongation of the alloy is in the range of 20.0%–21.8%.

Fig. 13d shows the changing curve of the conductivity. It can be found that there is a significant increase in conductivity after CR and aging, which continues to increase with aging time. The conductivity after CR is 47.4%IACS; after aging at 450 °C for 1 h, the conductivity is 76.8%IACS, which is 62.0% higher than that before aging. After that, the conductivity increases slowly with the aging time, and the conductivity increases to 82.5%IACS after aging for 4 h. After aging, the conductivity of the CuCrZr alloy shows a significant increase. This is due to the rearrangement or elimination of defects within the material during the aging process, the restoration of lattice distortion to a certain extent as well as the precipitation of atoms in the secondary phase, which reduces the electron scattering and increases the conductivity. Therefore, three-passes C-ECAP by Route A, 75% CR, and aging at 450 °C for 2 h are the optimum treatment conditions for Cu0.9Cr0.1Zr alloys, which reaches the tensile strength of 537 MPa and the conductivity of 80%IACS. Furthermore, as shown in Table 1, under the

Table 1 Comparison of mechanical properties and conductivity of CuCrZr alloy

Tensile strength/MPa	Conductivity/ %IACS	Microhardness/ HV	Ref.
412	88.4	116.9	[6]
549	30	165	[33]
393.5	88.8	148.7	[34]
446	85	151.7	[35]
494.27	80.6	155.6	[36]
538	82.5	168	This work

optimal process parameters, the high-strength and high-conductivity CuCrZr alloy prepared in this study has significant advantages compared to those prepared by other methods.

4 Conclusions

1) With the increase in deformation reduction, the grains are gradually elongated and fragmented noticeably along the direction of deformation, making the GBs indistinct. This process promotes the formation of micro-nano fibrous structures within the CuCrZr alloy.

2) Grains after CR break up more completely, and are more likely to rotate, which leads to an increase in the internal polar density of the alloy as CR reduction increases, and the texture continues to concentrate.

3) Three-passes C-ECAP by Route A, 75% CR, and aging at 450 °C for 2 h are the optimum treatment conditions for Cu0.9Cr0.1Zr alloy, resulting in the tensile strength of 537 MPa and the conductivity of 80%IACS.

References

1 Guo Tingbiao, Qian Danchen, Huang Dawei *et al. Journal of Central South University*[J], 2023, 30: 2094

2 Wang Yujian, Qu Jianping, Wang Xiaolong *et al. Journal of Alloys and Compounds*[J], 2022, 902: 12

3 Xia Chengdong, Zhang Wan, Kang Zhanyuan *et al. Materials Science and Engineering A*[J], 2012, 538: 295

4 Xu Gaolei, Peng Lijun, Huang Guojie *et al. Rare Metals*[J], 2021, 40(8): 2213

5 Bao Weizong, Yan Han, Chen Jie *et al. Materials Science and Engineering A*[J], 2021,825: 9

6 Han Fei, Jiang Yihui, Cao Fei *et al. Materials Characterization*[J], 2023, 199: 7

7 Li Wanli, Hu Dawei, Li Lingying *et al. ACS Applied Materials & Interfaces*[J], 2017, 9: 24711

8 Sun L X, Tao N R, Lu K. *Scripta Materialia*[J], 2015, 99: 73

9 Gholami M, Vesely J, Altenberger I *et al. Materials Science and Engineering A*[J], 2017, 684: 524

10 Zhang Xiaohui, Xiong Dingbang, Liu Yazhou *et al. Acta Materialia*[J], 2024, 267: 11

11 Zhang Zhefeng, Li Keqiang, Cai Tuo *et al. Acta Metallurguca Sinica*[J], 2023, 59: 467 (in Chinese)

12 Gao Yang, Guo Tingbiao, Feng Rui *et al. Materials Characterization*[J], 2024, 208: 12

13 Ladani L, Razmi J, Lowe T C. *Journal of Manufacturing and Materials Processing*[J], 2023, 7: 137

14 Purcek G, Yanar H, Saray O *et al. Wear*[J], 2014, 311: 149

15 Guo Tingbiao, Feng Rui, Li Kaizhe *et al. Rare Metal Materials and Engineering*[J], 2023, 52(7): 2396

16 Kovácová A, Kvackaj T, Kocisko R. *et al. Acta Physica Polonica A*[J], 2017, 131: 1336

17 Wei Kunxia, Wei Wei, Wang Fei *et al*. *Materials Science and Engineering A*[J], 2011, 528(3): 1478

18 Chu Zhuqi, Fan Zhen, Wei Wei *et al. Journal of Alloys and Compounds*[J], 2025, 1036: 181880

19 Su Juanhua, Dong Qiming, Liu Ping *et al. Materials Science and Engineering A*[J], 2005, 392: 422

20 Chen Xiaohong, Zhou Honglei, Zhang Tao *et al. Materials & Design*[J], 2019, 180: 107976

21 Sousa T G D, Pires W M, Cruz R B D *et al. Matéria (Rio de Janeiro)*[J], 2024, 29(2): e20230370

22 Hajizadeh K, Farhad H, Kurzydlowski K J. *Applied Physics A*[J], 2023, 129(8): 583

23 Stolyarov V V, Zhu Y T, Alexandrov I V *et al. Materials Science and Engineering A*[J], 2001, 299(1–2): 59

24 Shahmir H, Asghari-Rad P, Mehranpour M S *et al. Materials Science and Engineering A*[J], 2021, 807: 140875

25 Schuh C A, Lu K. *MRS Bulletin*[J], 2021, 46(3): 225

26 Singh B, Edwards D, Eldrup M *et al. Journal of Nuclear Materials*[J], 1997, 249(1): 1

27 Zhang Qifei, Tang Xiu, Liu Bin *et al. Journal of Materials Research and Technology*[J], 2023, 27: 7839

28 Purcek G, Yanar H, Demirtas M *et al. Journal of Alloys and Compounds*[J], 2020, 816: 152675

29 Li Longjian, Li Rengeng, Zhang Jiajun *et al. Acta Metallurgica Sinica*[J], 2022, 60(3): 405 (in Chinese)

30 Mao Weimin, Yang Ping, Chen Leng. *Principle and Detection Technology of Material Texture Analysis*[M]. Beijing: Metallurgical Industry Press, 2008 (in Chinese)

31 Shen Zhe, Lin Zhongze, Shi Peijian *et al. Journal of Materials Science & Technology*[J], 2022, 110: 187

32 Xin Zhao, Jiang Yanbin, Wu Zixiao *et al. Materials Characterization*[J], 2024, 207: 113557

33 Liang Ningning, Liu Jizi, Lin Sicong *et al. Journal of Alloys and Compounds*[J], 2018, 735: 1389

34 Li Qi, Liu Yahui, Zhu Qianqian *et al. Journal of Alloys and Compounds*[J], 2025, 1032: 181261

35 Li Qi, Liu Yahui, Zhu Qianqian *et al. Materials Science and Engineering A*[J], 2025, 937: 148360

36 Guo Tingbiao, Wang Huan, Qian Danchen *et al. Physics of Metals and Metallography*[J], 2024, 125: 1557

C-ECAP冷轧和时效热处理制备微纳高强高导电性Cu0.9Cr0.1Zr合金

郭廷彪[1,2]，李颖颖[1]，钱丹晨[1]，邓　阳[1]，张国庆[1,2]，王艳风[3]，李文兵[3]，凌得魁[3]

(1. 兰州理工大学 省部共建有色金属先进加工与再利用国家重点实验室，甘肃 兰州 730050)

(2. 兰州理工大学 有色金属合金及加工教育部重点实验室，甘肃 兰州 730050)

(3. 镍钴资源综合利用国家重点实验室，甘肃 金昌 737100)

摘　要：Cu0.9Cr0.1Zr合金通过A路径的连续等通道转角挤压（C-ECAP）变形，随后进行液氮低温轧制（CR），并进行450 ℃的时效处理。利用电子背散射衍射仪、能量色散光谱仪、X射线衍射仪、扫描电子显微镜和透射电子显微镜对合金的微观结构、力学性能和导电性能进行了检测，分析了变形过程中织构演变机制及其对性能的影响。结果表明，在C-ECAP过程中，CuCrZr合金的微观结构中形成了定向剪切带，且微观结构的择优取向与轧制方向一致。变形后，随着变形量的增加，合金中析出相（主要是Cr）的含量增加，并伴随着微纳结构纤维状组织的出现。经过3次C-ECAP挤压、75%冷轧变形以及在450 ℃下时效2 h后，合金的抗拉伸强度、硬度和电导率分别达到538 MPa、168 HV和80%IACS。低温轧制、时效热处理以及再结晶织构的形成均有利于提高合金的电导率。

关键词：连续等通道转角挤压（C-ECAP）；低温轧制；时效热处理；析出相；微纳结构

作者简介：郭廷彪，男，1974年生，博士，教授，兰州理工大学省部共建有色金属先进加工与再利用国家重点实验室，甘肃 兰州 730050，E-mail：guotb@lut.edu.cn